Acta Crystallographica Section D
Biological Crystallography
ISSN 0907-4449

Phase transition of triclinic hen egg-white lysozyme crystal associated with sodium binding

Kazuaki Harata* and Toshihiko Akiba

Biological Information Research Center, National Institute of Advanced Industrial Science and Technology, Central 6, 1-1-1 Higashi, Tsukuba, Ibaraki 305-8566, Japan

Correspondence e-mail: k-harata@aist.go.jp

Received 11 December 2003
Accepted 23 January 2004

PDB References: form I crystal, 1v7s, r1v7ssf; form II crystal, 1v7t, r1v7tsf.

A triclinic crystal of hen egg-white lysozyme obtained from a D_2O solution at 313 K was transformed into a new triclinic crystal by slow release of solvent under a temperature-regulated nitrogen-gas stream. The progress of the transition was monitored by X-ray diffraction. The transition started with the appearance of strong diffuse streaks. The diffraction spots gradually fused and faded with the emergence of diffraction from the new lattice; the scattering power of the crystal fell to a resolution of 1.5 Å from the initial 0.9 Å resolution. At the end of the transition, the diffuse streaks disappeared and the scattering power recovered to 1.1 Å resolution. The transformed crystal contained two independent molecules and the solvent content had decreased to 18% from the 32% solvent content of the native crystal. The structure was determined at 1.1 Å resolution and compared with the native structure refined at the same resolution. The backbone structures of the two molecules in the transformed crystal were superimposed on the native structure with root-mean-square deviations of 0.71 and 0.96 Å. A prominent structural difference was observed in the loop region of residues Ser60–Leu75. In the native crystal, a water molecule located at the centre of this helical loop forms hydrogen bonds to main-chain peptide groups. In the transformed crystal, this water molecule is replaced by a sodium ion with octahedral coordination that involves water molecules and a nitrate ion. The peptide group connecting Arg73 and Asn74 is rotated by 180° so that the CO group of Arg73 can coordinate to the sodium ion. The change in the X-ray diffraction pattern during the phase transition suggests that the transition proceeds at the microcrystal level. A mechanism is proposed for the crystal transformation.

1. Introduction

In unusual environments, for example low humidity or high pressure, protein crystals undergo changes in molecular arrangement and even in the protein structure itself (Kundrot & Richards, 1987; Madhusudan *et al.*, 1993). An orthorhombic crystal of ribonuclease A was dehydrated with $CaSO_4$ to 10% solvent content (Bell, 1999) and a structural change with an r.m.s. difference of 1.6 Å from the native structure was prominent in the surface-loop region. Dehydration of a monoclinic crystal of ribonuclease A at 79% relative humidity reduced the solvent content to 30.9% from the value of 43.4% in the native crystal (Kishan *et al.*, 1995). The r.m.s. difference in the C^{α}-atom position was 0.55 Å and a hinge-bending movement of the two domains was observed. In contrast, a small loss of solvent (1.6% of the unit-cell volume) from a tetragonal crystal of hen lysozyme did not significantly affect the protein structure (Kodandapani *et al.*, 1990).

A phase transition induced by dehydration has been observed in a monoclinic crystal of hen egg-white lysozyme (Madhusudan *et al.*, 1993). The native crystal contains two independent molecules in the asymmetric unit, with 32% solvent content. At 88% relative humidity, the crystal was transformed into another monoclinic crystal form that contains one molecule in the asymmetric unit and has 22% solvent content. Even in a crystal with 9.4% solvent content, the protein molecule essentially retains the same backbone structure as that of the native crystal, with an r.m.s. deviation of 0.96 Å for C^{α} atoms (Nagendra *et al.*, 1998). Dobrianov *et al.* (1999) have investigated the change in crystal habit using X-ray topography. Controlled dehydration of tetragonal hen lysozyme showed the crystal to be largely unchanged for 24 h at 81% relative humidity and to suddenly degrade after 31 h. They have suggested that during water removal the lysozyme molecules remain in an ordered metastable configuration, stabilized by crystal contacts, before undergoing conformational changes and/or displacements and rotations in the unit cell.

We have found that on dehydration the triclinic crystal of hen lysozyme undergoes a phase transition, producing a crystal with a new lattice, and have succeeded in following the progress of the transformation by means of single-crystal X-ray diffraction. The changes in the X-ray diffraction images during the phase transition were recorded and the structure of the transformed crystal was determined at atomic resolution. In the present paper, we report this new finding and discuss the mechanism of the phase transition and the dynamic change in the protein structure.

2. Materials and methods

Triclinic crystals of hen egg-white lysozyme (Seikagaku Kogyo Co.) were obtained from a D_2O solution containing 1%(*w*/*v*) protein, 2%(*w*/*v*) sodium nitrate and 10 m*M* sodium acetate. The protein solution (pD 4.5) to which seed crystals were added was allowed to stand at 313 K. Crystals grew in two weeks; the temperature was then gradually lowered to room temperature. X-ray diffraction experiments were carried out on a Bruker SMART6000 diffractometer with Cu $K\alpha$ radiation from a MAC Science M06X rotating-anode generator (50 kV, 90 mA, focal spot size 0.3 mm) equipped with Osmic Confocal Max-Flux Optics. Intensity data from the native crystal (form I) sealed in a glass capillary with a small amount of mother liquor were collected at 290 K. Two crystals were used for data collection to 1.1 Å resolution. For measurement of the phase transition, the crystal was immersed in paraffin oil (Hampton Research) and the visible solvent was carefully removed. The crystal in an oil drop was picked up in a cryo-loop and placed in a temperature-regulated nitrogen-gas stream. X-ray diffraction images were recorded at 263 K during the phase transition, which was completed in 17 h. The temperature was then quickly lowered to 90 K and the intensity data of the new crystal (form II) were collected to 1.1 Å resolution.

Table 1
Summary of data collection and structure refinement.

	Form I	Form II
Data collection		
Crystal system	Triclinic	Triclinic
Space group	*P*1	*P*1
Unit-cell parameters		
a (Å)	27.23 (1)	25.84 (3)
b (Å)	31.97 (2)	39.96 (4)
c (Å)	34.27 (2)	42.53 (4)
α (°)	88.44 (4)	88.07 (5)
β (°)	108.62 (4)	95.76 (5)
γ (°)	111.71 (5)	90.80 (5)
Z	1	2
V_M (Å^3 Da^{-1})	1.80	1.51
Temperature (K)	290	90
Resolution range (Å)	17.09–1.14	39.94–1.13
No. observed reflections	127736	165394
No. unique reflections	36551	52044
R_{merge}	0.038	0.034
Completeness	0.956	0.806
Structure refinement		
No. of reflections	36551	52044
Resolution range	17.09–1.14	39.94–1.13
No. parameters	10794	20892
R value (all data)	0.090	0.119
R_{free} value (5% data)	0.120	0.146
Residual density (min/max) (e Å^{-3})	−0.40/0.41	−0.40/0.54

The structure of the form II crystal was solved by molecular replacement using *X-PLOR* (Brünger, 1992) and the structure of the triclinic crystal (Ramanadham *et al.*, 1990; PDB code 2lzt) as an initial model. In the refinement using *SHELX*97 (Sheldrick, 1997), isotropic temperature factors were used in the initial stage and anisotropic temperature factors were then introduced stepwise in the order main-chain atoms, side-chain atoms and solvent atoms. The conjugate-gradient algorithm was used to solve the simultaneous equation. H-atom coordinates were calculated and included in the structure-factor calculation with an isotropic temperature factor that was 1.2 or 1.5 times larger than that of the bonded non-C or C atoms, respectively. Electron-density peaks higher than 0.25 e Å^{-3} were considered to be solvent atoms. Pairs of solvent peaks at a distance of less than 2.5 Å were treated as disorder. The occupancy factors of solvent molecules were refined once for atoms with no significant shift in atomic parameters and then fixed in subsequent calculations. After solvent molecules had been picked and disordered side-chain groups had been reasonably modelled, block-matrix least-squares calculation was adopted for two protein molecules and a set of solvent molecules containing water and sodium nitrate. The refinement of the form I crystal was performed using the same procedure. A full-matrix least-squares calculation was performed at the final stage. The statistics of data collection and structure refinement are given in Table 1.

3. Results

3.1. Measurement of the phase transition by X-ray diffraction

The triclinic crystal (form I) was transformed to another triclinic crystal (form II) by exposure to a dry nitrogen-gas

stream at 263 K. The V_M value (Matthews, 1968) indicated that the solvent content had decreased from 32 to 18% during the transition. During the X-ray diffraction measurement, the crystal in the cryoloop was coated with paraffin oil. The solvent in and around the crystal was slowly released through the paraffin coat under the dry nitrogen-gas stream. The phase transition was detected by consecutive measurements of the X-ray diffraction. The crystal was kept at 283 K until the transition started; the temperature was then lowered to 263 K to record the transition process. The relatively fast release of solvent at 283 K not only accelerated the transition but also caused deterioration of the crystal. Below 263 K, the phase transition proceeded so slowly that X-ray diffraction images could be recorded for more than 10 h.

Fig. 1 shows the change in two sets of X-ray diffraction images that were recorded for 1.0° rotation around the ω axis. One set was measured at $\varphi = 0°$ (series A in Fig. 1) and the other at $\varphi = 90°$ (series B). In the initial stage of the transition, strong diffuse streaks appeared. As the transition proceeded, the diffraction spots gradually fused and small but sharp diffraction spots from the new lattice appeared in the low-resolution area (A-2). At this stage, the scattering power fell to about 1.5 Å resolution. As the new diffraction spots developed, the diffuse diffraction spots from the original lattice became weaker and weaker. The reflections from the form II crystal were approximately doubled in number, as the new unit cell contained two independent molecules. In the final stage of the phase transition, the diffuse streaks slowly disappeared and the scattering power of the crystal recovered to 1.1 Å resolution (A-3).

3.2. Structure determination and refinement

After the phase transition was complete, the temperature was lowered to 90 K and intensity data from the form II crystal were collected to 1.1 Å resolution. Data collection at 263 K was not successful because the crystal gradually deteriorated by continuous release of solvent through the paraffin coat. The unit-cell volume of the form II crystal was 1.67 times larger than the volume of the form I crystal, but the V_M value was reduced by 16.4% as the new unit cell contains two protein molecules.

The structure was solved by molecular replacement using a set of coordinates for triclinic lysozyme (Ramanadham *et al.*,

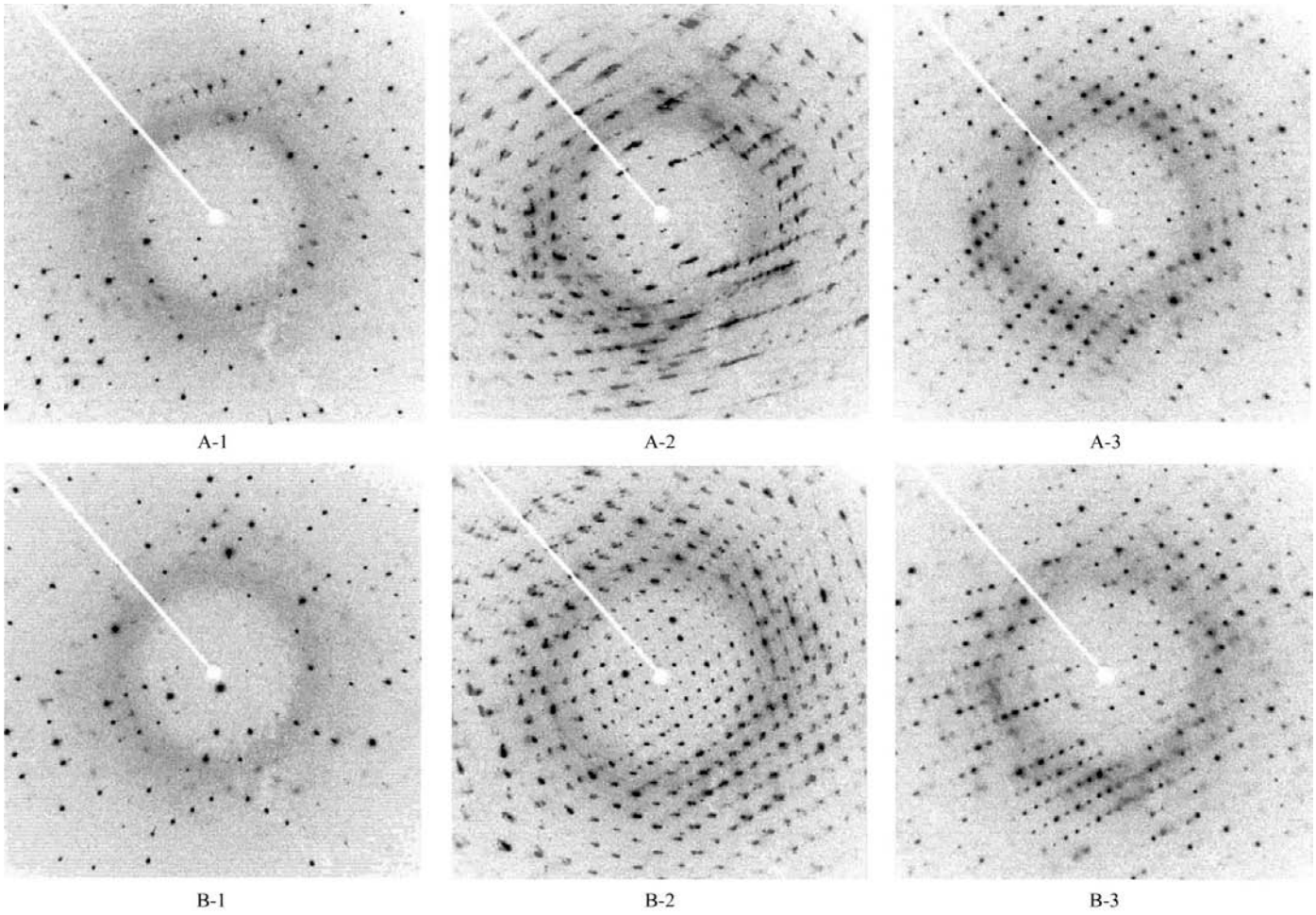

Figure 1
X-ray diffraction images of the phase transition recorded for 60 s exposure with 1° rotation. The crystal-to-detector distance was 55 mm and a 0.3 mm collimator was used. The A series are images taken at $\varphi = 0°$ and the B series at $\varphi = 90°$. The numbers from 1 to 3 correspond to images taken before the transition, during the transition and after the transition, respectively.

Table 2
Intermolecular polar contacts less than 3.3 Å.

(*a*) Form I crystal.

Contact	Distance (Å)	Symmetry code
Phe3 O–Arg73 NH1	3.24	*c*
Glu7 OE2–Lys97 NZ	3.00	*c*
Glu7 OE2–Asp101 OD2	2.57	*c*
Arg14 O–Asn37 ND2	3.13	*b*
Gly16 O–Arg114 NH1	2.86	*b*
Gly16 O–Arg114 NH2	3.14	*b*
Asp18 O–Arg114 NH2	3.01	*b*
Asn19 ND2–Ser81 O	2.99	*f*
Arg21 O–Arg68 NH2	2.95	*f*
Arg21 NH2–Asp66 O	2.92	*f*
Arg45 O–Asn77 ND2	2.95	*e*
Gly67 O–Gly126 N	3.12	*k*
Asn77 OD1–Lys116 NZ	2.85	*h*
Ser81 OG–Asn113 O	3.30	*h*

(*b*) Form II crystal.

	Distance (Å)	Symmetry code
Arg14_1 O–Asn37_1 ND2	2.50	*b*
Gly16_1 O–Arg114_1 NH1	2.77	*b*
Gly16_1 O–Arg114_1 NH2	2.90	*b*
Asp18_1 O–Arg114_1 NH2	2.83	*b*
Asn44_1 OD1–Lys97_1 NZ	3.09	*e*
Asn46_1 ND2–Lys97_1 NZ	3.17	*e*
Gly71_1 O–Arg125_1 NH1	2.75	*d*
Ser72_1 OG– Ala122_1 O	3.07	*d*
Arg73_1 NH1–Arg125_1 NH2	3.15	*d*
Arg73_1 NH2–Asp119_1 OD1	2.88	*d*
Asn74_1 O–Arg128_1 NH1	3.08	*d*
Asn77_1 OD1–Arg128_1 NE	2.89	*b*
Arg14_2 O–Asn37_2 ND2	2.93	*b*
Gly16_2 O–Arg114_2 NH1	2.89	*b*
Asp18_2 O–Arg114_2 NH1	3.08	*b*
Arg21_2 NE–Asn113_2 OD1	2.98	*b*
Asn44_2 ND2–Asn93_2 OD1	3.18	*e*
Asn46_2 O–Asn77_2 ND2	2.86	*e*
Thr47_2 OG1–Leu75_2 O	2.85	*e*
Asn65_2 OD1–Gly126_2 N	2.99	*d*
Lys1_1 NZ–Leu129_2 OXT	2.50	*d*
Arg14_1 NH2–Asp101_2 O	2.96	*b*
Asp18_1 OD1–Gln41_2 OE1	3.00	*h*
Asn19_1 OD1–Gln41_2 OE1	2.84	*h*
Asn19_1 ND2–Leu84_2 O	3.14	*h*
Arg21_1 O–Arg68_2 NH1	2.83	*h*
Arg21_1 O–Arg68_2 NH2	2.80	*h*
Arg21_1 NH2–Asp66_2 O	2.79	*h*
Tyr23_1 OH–Arg68_2 NE	3.24	*h*
Asn27_1 OD1–Arg45_2 NH2	3.04	*h*
Asn37_1 O–Arg73_2 NH1	3.03	*a*
Asn37_1 O–Arg73_2 NH2	2.80	*a*
Asn37_1 OD2 –Arg73_2 NH1	2.70	*a*
Gln41_1 OE1–Asn19_2 ND2	2.87	*d*
Asp48_1 N–Val2_2 O	3.12	*j*
Arg61_1 NH1–Ser86_2 O	3.27	*j*
Arg61_1 NH2–Ser86_2 O	2.95	*j*
Arg68_1 NE– Tyr23_2 OH	3.24	*d*
Arg68_1 NH1–Arg21_2 O	2.81	*d*
Arg73_1 NH2–Thr89_2 OG1	2.98	*j*
Asn77_1 OD1–Lys116_2 NZ	2.90	*i*
Ser81_1 OG–Asn113_2 O	2.76	*i*
Leu84_1 O–Asn19_2 ND2	3.27	*d*
Asp87_1 OD2–Asp119_2 N	2.58	*i*
Ser100_1 O–Arg5_2 NE	3.24	*l*
Ser100_1 O–Arg5_2 NH2	2.75	*l*
Asp101_1 O–Arg14_2 NH1	3.23	*j*
Asn106_1 O–Arg128_2 NH1	3.20	*j*
Arg112_1 NE–Cys127_2 O	2.90	*j*
Arg112_1 NH1–Leu129_2 N	2.78	*j*
Asn113_1 O–Ser81_2 OG	2.46	*c*
Asn113_1 ND2–Gly126_2 O	3.09	*j*
Lys116_1 NZ–Asn77_2 OD1	2.96	*c*
Asp119_1OD1–Asp87_2 OD1	2.49	*c*
Gln121_1 OE1–Gln41_2 NE2	2.79	*h*
Arg125_1 NH2 –Asn39_2 OD1	3.23	*h*
Arg128_1 O–Asn103_2 ND2	2.85	*b*

Symmetry operators: (*a*) x, y, z; (*b*) $x-1, y, z$; (*c*) $x, y-1, z$; (*d*) $x, y, z-1$; (*e*) $x+1, y, z$; (*f*) $x, y+1, z$; (*g*) $x, y, z+1$; (*h*) $x-1, y-1, z$; (*i*) $x-1, y, z-1$; (*j*) $x, y-1, z-1$; (*k*) $x, y-1, z+1$; (*l*) $x-1, y-1, z-1$.

1990) and refined by the least-squares method. In the structure refinement, block-matrix least-squares calculation was adopted for each protein molecule and a set of solvent molecules. The statistics of the structure refinement, which converged at an R value of 0.119 for all reflections, are given in Table 1. The final structure model contained two lysozyme molecules, two sodium ions, five nitrate ions and D_2O molecules distributed over 223 sites. The average e.s.d. of the atomic coordinates was 0.026 Å for all atoms including solvent atoms and 0.017 Å for main-chain peptide atoms.

To compare the protein structures before and after the phase transition, intensity data from the form I crystal were also collected to 1.1 Å resolution at 290 K. The full-matrix least-squares refinement converged to an R value of 0.090 for all reflections. The structure contained one protein molecule, seven nitrate ions and D_2O molecules distributed over 161 sites. The average e.s.d. of the atomic coordinates was 0.022 Å for all atoms including solvent atoms and 0.010 Å for main-chain peptide atoms.

3.3. Crystal structure

The crystal packing before and after the phase transition is shown in Fig. 2. Intermolecular polar contacts of less than 3.3 Å are listed in Table 2. It is obvious that the molecules in the form II crystal are more densely packed than those in the form I crystal. The number of amino-acid residues involved in intermolecular polar contacts between protein molecules increased from 23 in the form I crystal to 44 (molecule 1) and 42 (molecule 2) in the form II crystal. The two molecules in the form II crystal are related by the equations

$$X' = 0.9970X - 0.0600Y + 0.0488Z + 16.260,$$
$$Y' = 0.0556X + 0.9947Y + 0.0861Z + 21.747,$$
$$Z' = -0.0538X - 0.0832Y + 0.9951Z + 22.338.$$

These molecules are nearly in the same orientation and can be superimposed by a rotation of 0.5° and translation along the three lattice axes.

3.4. Molecular structure

The two independent molecules in the form II crystal were superimposed with an r.m.s.d. of 0.76 Å for equivalent C^{α} atoms. A significant deviation was observed in the regions

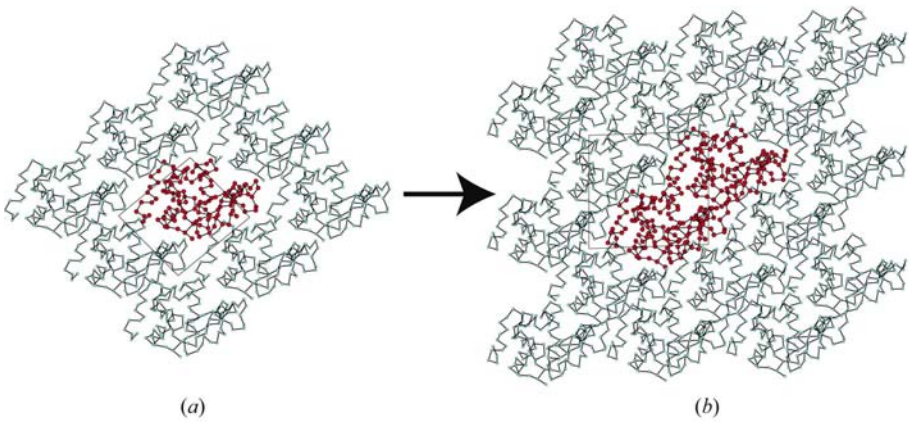

Figure 2
Crystal packing of the native crystal (*a*) and the transformed crystal (*b*). The structures are viewed along the *a* axis. The independent molecules in the asymmetric unit are shown in a red colour. The transformed crystal contains two molecules in the unit cell.

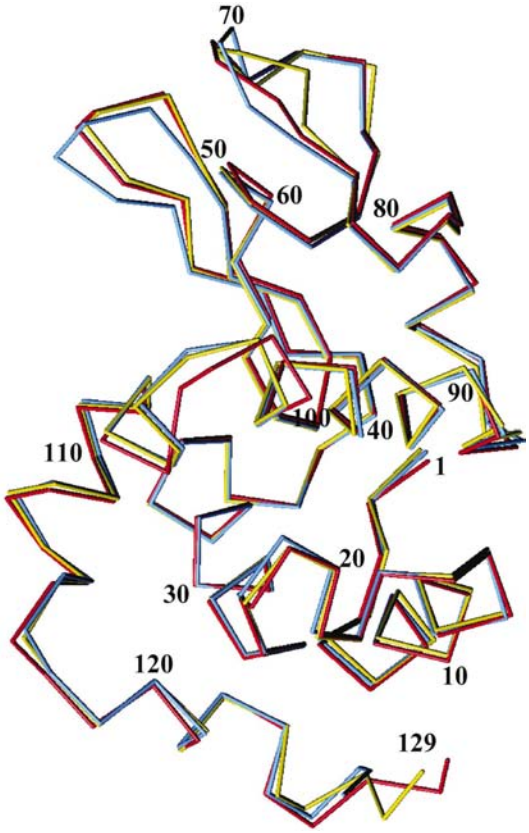

Figure 3
Superposition of molecule 1 (yellow) and molecule 2 (blue) in the transformed crystal on the molecule (red) in the native crystal. The r.m.s. difference between molecules 1 and 2 is 0.76 Å and the difference from the native molecule is 0.71 Å for molecule 1 and 0.96 Å for molecule 2.

Arg45–Gly49 (type I β-turn), Pro70–Arg73 (type II β-turn) and Arg128–Leu129 (C-terminus). A structural difference in these regions was also observed in the comparison with the form I crystal. Fig. 3 shows the superposition of the two molecules in the form II crystal on the molecule in the form I crystal with r.m.s.d. values of 0.71 and 0.96 Å. Relatively large differences in the backbone structure between the form I and form II crystals were observed in the region of residues Val99–Gly104. In both the molecules in the form II crystal a type II′ β-turn was observed for residues Asn103–Asn106, while residues Gly104–Ala107 in the form I crystal form a type III β-turn.

Fig. 4 shows the anisotropic motion of the C^{α} atoms. The average B_{eq} values for the form I crystal at 290 K are 13.1 Å^2 for all atoms including those of solvent molecules and 10.7 Å^2 for the main-chain peptide atoms. In contrast, the corresponding values for the form II crystal at 90 K are 13.7 and 11.5 Å^2 for molecule 1 and 15.5 and 13.4 Å^2 for molecule 2, respectively. The relatively large B_{eq} values in the form II crystal even at low temperature indicate that the structure is not as ordered as that of the native crystal. The mode of structural fluctuation is not identical for the two independent molecules. Molecule 1 shows large B_{eq} values in the region of residues Ser85–Asp87 and Ser100–Asn103. Large B_{eq} values are observed in the region of residues Arg45–Gly49 and Arg125–Leu129 in molecule 2.

3.5. Sodium binding

The most prominent structural change associated with the phase transition is observed in the region of residues Ser60–Leu75. This region forms a large helical loop structure. In the form I crystal, one water molecule located inside the loop stabilizes the structure by forming hydrogen bonds to three peptide O atoms (Ser60 O, Arg61 O and Cys64 O), the OG—H hydroxyl group of Ser72 and the NH group of Asn74. This water molecule is replaced with a sodium ion in the form II crystal as shown in Fig. 5. In both of the molecules, six O atoms are coordinated to the sodium ion, thus forming a distorted octahedral structure (Fig. 6). Three carbonyl O atoms, Ser60 O, Cys64 O and Arg72 O, are coordinated to the sodium ion in both molecules. Two O atoms of the nitrate ion are directly coordinated in molecule 1. In molecule 2, they are replaced with water molecules that are hydrogen bonded to a nitrate ion. The hydroxyl O atom of Ser72 is coordinated in molecule 2. However, in molecule 1 this hydroxyl group points away from the sodium ion and a water molecule occupies the position.

The peptide bond linking residues Arg73–Asn74 is rotated by about 180° after the phase transition. The NH group of Asn74 is hydrogen bonded to a water molecule in the form I crystal, but the carbonyl O atom of Arg73 is coordinated to the sodium ion in the form II crystal. The (φ, ψ) angles of the 73rd and 74th residues in the form I crystal are (−104.6, −25.6) and (46.3, 55.6), respectively. In contrast, the corresponding angles in molecule 1 of the form II crystal are (−84.6, 147.0) and (−152.0, 67.3), respectively.

4. Discussion

The structure of protein crystals is largely maintained by a limited number of protein–protein contacts, while solvent molecules fill the intermolecular space. On dehydration of protein crystals, changes in the molecular and crystal structure are expected to compensate for the effect of loss of bulk solvent. The phase transition is a plausible process by which the crystal can adapt to the environmental change when the crystal lattice can no longer stand it. The crystals produced by the phase transition showed a molecular structure and crystal packing with characteristics that were not observed in the native state (Madhusudan *et al.*, 1993). By the phase transition, the form I crystal of hen lysozyme was transformed to another triclinic crystal containing two independent molecules. Steinrauf (1998) determined the structure of a triclinic crystal of hen lysozyme (PDB code 1lks) that contains two independent molecules. However, its crystal packing (space group *A*1) differs from the form II crystal. The form I crystal was obtained from a D_2O solution. We have previously reported that D_2O is a better solvent than H_2O for the crystallization of human α-lactalbumin (Harata *et al.*, 1999). The result of the structure refinement of the form I crystal (Table 1) indicates that D_2O is also a good solvent for hen egg-white lysozyme.

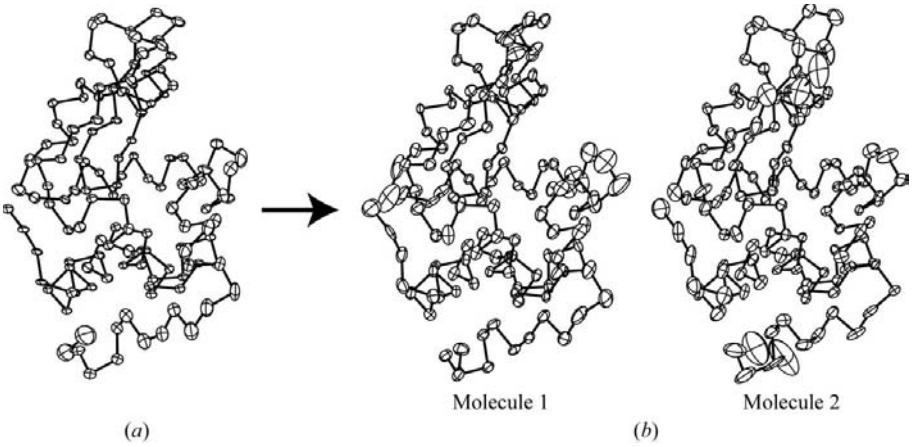

Figure 4
Comparison of the anisotropic thermal motion of C^{α} atoms between the native crystal (*a*) and the transformed crystal (*b*). The thermal ellipsoids are drawn with 75% probability.

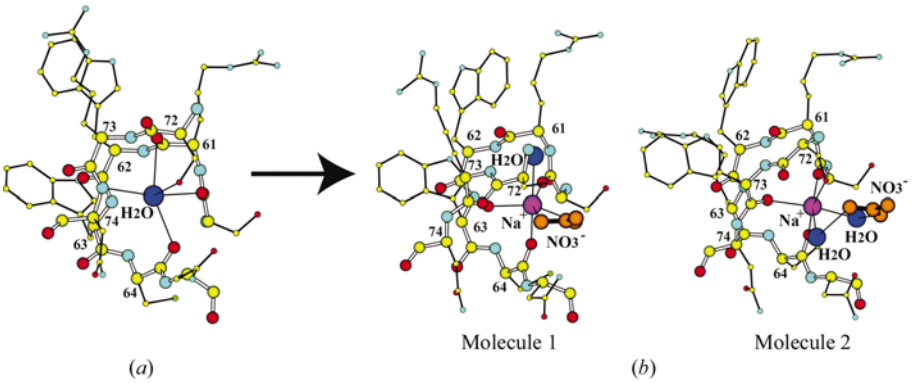

Figure 5
Structure of the sodium-binding site in the native crystal (*a*) and the transformed crystal (*b*). The water molecule in the native crystal is replaced by a sodium ion in the transformed crystal. In molecule 1 a nitrate anion is directly coordinated, but in molecule 2 a nitrate ion is bound by water-mediated hydrogen bonds.

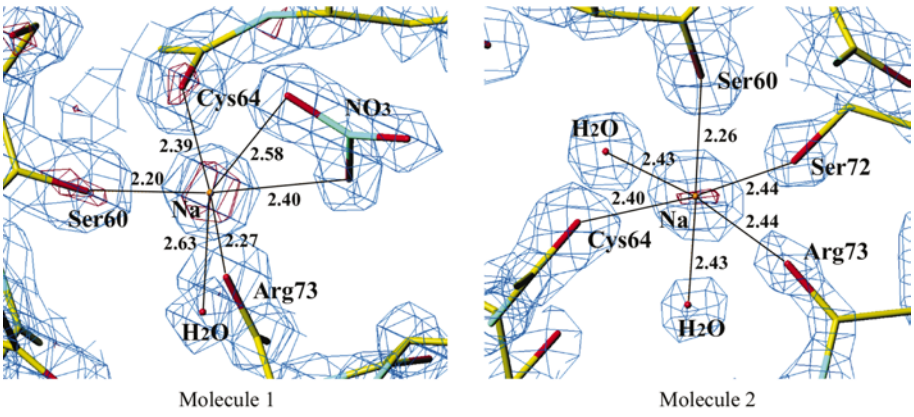

Figure 6
$3F_o - 2F_c$ electron-density maps of the sodium-binding sites. Contours are drawn at the 2σ level (blue) and 5σ level (red).

The phase transition induced by the dehydration starts abruptly when the solvent content becomes critical, although there may be a metastable state before the transition occurs (Dobrianov *et al.*, 1999). When the crystal in an oil drop was mounted on a cryoloop for measurement of X-ray diffraction, the crystal was still covered with a thin layer of mother liquor under the paraffin coat. The release of the bulk solvent from the crystal should be delayed until the mother liquor had gone from the crystal surface. The phase transition took some 10 min or several hours depending on the amount of mother liquor on the crystal surface, the thickness of the paraffin coat and the crystal size. The transformation of a small crystal was so fast at the room temperature that it was difficult to record the change in the diffraction images. Our attempts have shown that the rate of transformation can be controlled by the regulation of temperature as the release of solvent is more suppressed at the lower temperature. In the temperature range 243–263 K, the phase transition took several hours and hundreds of X-ray diffraction images could be recorded.

Loss of bulk solvent should induce rearrangement of protein and solvent molecules to reduce the vacant space previously occupied by the released solvent. After the phase transition, the *a*-axis length was shortened by 1.4 Å and the volume per molecule was decreased by 16.1%. It is surprising that the crystal, which had dimensions larger than 0.5 mm, maintained its outward form without forming cracks during the phase transition. An intense increase in the mosaicity in the diffraction spots was observed in the early stages of the transition. The strong diffuse streaks observed during the phase transition indicate the lattice defect was caused by non-periodic displacement and/or movement of protein molecules in the crystal. These results suggest that the phase transition occurs at the level of microcrystals, tiny blocks that constitute the crystal.

A possible mechanism for the crystal transformation is illustrated in Fig. 7. When the solvent content reaches the critical amount, phase transition spontaneously occurs in some microcrystals to form nuclei of the new crystal, from which the transition propagates over the crystal. The transformed microcrystals cause defects in the crystal, which are responsible for the diffuse streaks in the X-ray diffraction. In the intermediate state, the crystal consists of two types of microcrystals, one with the old lattice and the other with the new lattice. The X-ray diffraction patterns (A-2 and B-2 in Fig. 1) clearly show the presence of both types of lattice in the intermediate state. The disordered alignment of these mixed microcrystals reduces the scattering power of the crystal to ∼1.5 Å resolution. However, when most of the microcrystals are transformed, they recover an ordered alignment and the scattering power is restored to 1.1 Å resolution.

The protein molecules change their local structure in cooperation with the lattice transformation in the microcrystal. In particular, a structural change in the protein surface may be required for the protein molecule to be accommodated in the transformed lattice. The transformation to the new lattice is accompanied by the release of a large amount of solvent (∼45% of the initial amount). The loss of bulk solvent with a large dielectric constant reduces the shielding effect against the electrostatic field originating from ionic side-chain groups. In addition to the packing problem caused by the solvent loss, enhancement of the electrostatic interaction between protein molecules may be a driving force for the molecular rearrangement. It is noteworthy that the phase transition is accompanied by sodium binding to the loop region of residues Ser60–Asn74. The loss of solvent increases the concentration of solute ions in the crystal. This may drive the binding of the sodium ion and induce a local conformational change that accelerates the reorganization of the crystal lattice. A similar sodium-binding structure has been observed in the tetragonal crystal obtained from a solution containing sodium chloride as precipitant (Vaney *et al.*, 1996). The conformational change itself may be independent of the phase transition, as both the water-bound conformer and sodium-bound conformer have also been found in the tetragonal crystal (Sauter *et al.*, 2001). However, the present results indicate that the sodium-bound conformer is more stable in the form II crystal than the water-bound conformer.

A nitrate ion is hydrogen bonded to two water molecules that are coordinated to the sodium ion bound to molecule 2 in the form II crystal. A similar binding of an anion is observed in the tetragonal crystal, where a chloride ion forms a hydrogen bond with a water molecule coordinated to the sodium ion (Sauter *et al.*, 2001). In contrast, a nitrate ion is directly coordinated to the sodium ion in molecule 1. In the form I crystal, a water molecule, D_2O, is bound to the position corresponding to the sodium binding in the same manner as observed in the triclinic crystal obtained from the H_2O solution (Walsh *et al.*, 1998). In the form I crystal, the NH group of Arg73 is hydrogen bonded to the water molecule. However, in the form II crystal, the peptide group linking Arg73 and Asn74 is rotated by 180° and the carbonyl O atom is coordinated to the sodium ion. To attain such a rotation of the peptide group, several residues need to move concertedly and this local structural change may be coupled with the movement of the whole molecule. Residues Arg73–Ile78 of the form I crystal form a wound sheet-like structure with residues Arg61–Asn65. The four NH–O hydrogen bonds Arg73–Arg61, Asn74–Trp62, Leu75–Trp63 and Ile78–Asn65 stabilize the structure of this region as well as the hydrogen bonds to the trapped water molecule. The flip of the peptide bond of residues Arg73–Asn74 breaks the sheet-like structure; instead, the sodium coordination stabilizes the conformation of the loop region. This structural change affects the conformational flexibility of the side chain of Trp62, which is the residue responsible for the substrate binding. In the form I crystal, the indolyl group of Trp62 is stacked on the side-chain group of Arg73. The loss of this stacking interaction in the form II crystal increases the flexibility of the side chain of Trp62, which is disordered in both the molecules. Such a conformational change may affect the binding of substrate sugars, although the effect on the enzyme action is unknown.

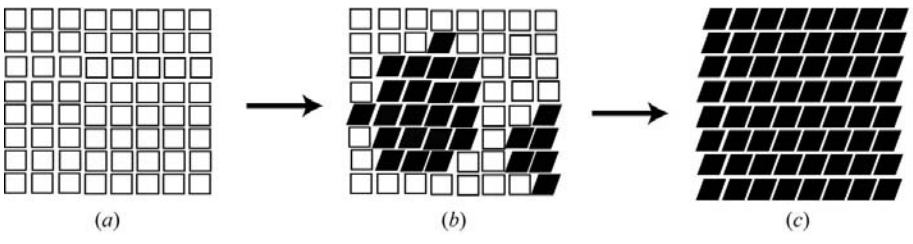

Figure 7
A possible mechanism for the phase transition. (*a*) The crystal consists of microcrystals shown by open squares. (*b*) When the solvent content reaches the critical amount, some microcrystals transformed to the new lattice to form nuclei, shown by full squares, from which the phase transition propagates over the crystal. (*c*) The new crystal is formed when all the microcystals are transformed.

The comparison of the thermal parameters between the form I and form II crystals shows the change of protein motion in the transformed crystal (Fig. 4). The average B_{eq} value of the form I crystal is smaller than that of the form II crystal, even though the

former structure was determined at 290 K and the latter at 90 K. Relatively large B_{eq} values in the form II crystal are observed in the region of residues Ser85–Asp87 and Ser100–Asn103 in molecule 1, while in molecule 2 the regions containing residues Arg45–Gly49 and Arg125–Leu129 have large B_{eq} values. Therefore, the molecular structure seems to be highly flexible during the phase transition and the variability still remains to some extent after the transformation. The apparently large thermal parameters of the from II crystal even at 90 K may be ascribed to the small disorder of side-chain groups, local structures and the molecule itself; in other words, the crystal is likely to consist of molecules with slightly different structures that cannot be resolved in the electron-density map. The high fluctuation of the protein structure in the form II crystal is also suggested by the intense diffuse scattering in the X-ray diffraction images A-3 and B-3 in Fig. 1, compared with the images A-1 and B-1 of the native state. The diffuse scattering is caused by rigid-body motion (Pérez *et al.*, 1996) and fluctuation of the protein structure (Clarage *et al.*, 1992). Consequently, the structure in the form II crystal is less ordered than that in the form I crystal.

This work was supported in part by the New Energy and Industrial Technology Development Organization (NEDO).

References

Bell, J. A. (1999). *Protein Sci.* **8**, 2033–2040.

Brünger, A. T. (1992). *X-PLOR. Version 3.1. A System for X-ray Crystallography and NMR.* Yale University, Connecticut, USA.

Clarage, J. B., Clarage, M. S., Phillips, W. C., Sweet, R. M. & Caspar, L. D. (1992). *Proteins*, **12**, 145–157.

Dobrianov, I., Caylor, C., Lemay, S. G., Finkelstein, K. D. & Thorne, R. E. (1999). *J. Cryst. Growth*, **196**, 511–523.

Harata, K., Abe, Y. & Muraki, M. (1999). *J. Mol. Biol.* **287**, 347–358.

Kishan, K. V. R., Chandra, N. R., Sudarsanakumar, C., Suguna, K. & Vijayan, M. (1995). *Acta Cryst.* D**51**, 703–710.

Kodandapani, R., Suresh, C. G. & Vijayan, M. (1990). *J. Biol. Chem.* **265**, 16126–16131.

Kundrot, C. E. & Richards, F. M. (1987). *J. Mol. Biol.* **193**, 157–170.

Madhusudan, R., Kodandapani, R. & Vijiayan, M. (1993). *Acta Cryst.* D**49**, 234–245.

Matthews, B. W. (1968). *J. Mol. Biol.* **33**, 491–497.

Nagendra, H. G., Sukumar, N. & Vijayan, M. (1998). *Proteins*, **32**, 229–240.

Pérez, J., Fauer, P. & Benout, J.-P. (1996). *Acta Cryst.* D**52**, 722–729.

Ramanadham, M., Sieker, L. C. & Jensen, L. H. (1990). *Acta Cryst.* B**46**, 63–69.

Sauter, C., Otálora, F., Gavira, J.-.A., Vidal, O., Giegé, R. & García-Ruiz, J. M. (2001). *Acta Cryst.* D**57**, 1119–1126.

Sheldrick, G. M. (1997). *SHELXL97. Program for Crystal Structure Refinement.* University of Göttingen, Germany.

Steinrauf, L. K. (1998). *Acta Cryst.* D**54**, 767–779.

Vaney, M. C., Maignan, S., Riès-Kautt, M. & Ducruix, A. (1996). *Acta Cryst.* D**52**, 505–517.

Walsh, M. A., Schneider, T. R., Sieker, L. C., Dauter, Z., Lamzin, V. S. & Wilson, K. (1998). *Acta Cryst.* D**54**, 522–546.